Supporting Information

# Simple fabrication of carbon quantum dots and activated carbon from waste wolfberry stems for detection and adsorption of copper ion

Yunjia Xu[1], Jingming Lan[1], Baoying Wang[1], Chunmiao Bo[1], Junjie Ou[2], Bolin Gong[1*]

[1]School of Chemistry and Chemical Engineering, Key Laboratory for Chemical Engineering and Technology, State Ethnic Affairs Commission, North Minzu University, Yinchuan, 750021, China

[2]State Key Laboratory of Synthetic and Natural Functional Molecule Chemistry of Ministry of Education, College of Chemistry & Materials Science, Northwest University, Xi'an 710127, China

***Corresponding author.**

**Email address:** gongbolin@163.com (B. Gong)

# Table of contents



## Experiment details

### Preparation of $Cu^{2+}$ chromogenic agent

A mother solution of $Cu^{2+}$ (1 mmol $L^{-1}$) was prepared by dissolving a certain amount of $CuSO_4$ $H_2O$ in water for subsequent experiments. An aqueous solution of

sodium diethyl dithiocarbamate (10 mg $mL^{-1}$) was prepared under dark conditions and labeled as a copper reagent, and a starch indicator, $NH_4Cl$-$NH_3 \cdot H_2O$ buffer solution (pH=9.25), was configured. Finally, the absorbance of 452 nm was measured to obtain the standard curve of $Cu^{2+}$ in the range of 10-50 μmol $L^{-1}$.

**Adsorption ability of wolfberry stem AC for metal ions**

In order to study the adsorption characteristics of wolfberry stem AC on $Cu^{2+}$, AC was added to the water sample containing $Cu^{2+}$, the adsorbed after $Cu^{2+}$ concentration was measured by UV spectrophotometer.

For isothermal adsorption experiments, AC (10 mg) was immersed in 200 mL of conical flasks containing different concentrations of $Cu^{2+}$ concentrations (100-240 μmol $L^{-1}$). The conical flask was placed on a 250 rpm thermostatic shaker and shaken for 3 h. The adsorbed $Cu^{2+}$ concentration was detected by UV spectrophotometer. The adsorption amount was calculated according to equation S(1)

$$Q_e=V(C_0-C_e)/m \qquad \text{S(1)}$$

where $V$ (L) is the solution volume, $C_0$ and $C_e$ (mg $L^{-1}$) are the initial and equilibrium metal ion concentrations in solution, $m$ (g) is the mass of adsorbent.

The isothermal adsorption curves were plotted by the adsorption capacity of AC at different $Cu^{2+}$ concentrations ($Q_e$) versus the initial concentration of $Cu^{2+}$ solution ($C_e$) (as ordinate). The isothermal adsorption curves of $Cu^{2+}$ were calculated used the Langmuir model equation S(2) and the Freundlich model equation S(3).

The Langmuir isotherm equation is given by the following:

$$C_e/Q_e=C_e/Q_{max}+1/K_LQ_{max} \qquad \text{S(2)}$$

$$\ln Q_e=\ln K_f+1/n \ln C_e \qquad \text{S(3)}$$

where $Q_{max}$ (mg $g^{-1}$) is the maximum adsorption capacity, $K_f$ (mg $g^{-1}$) and $K_L$ (L $mg^{-1}$) are the Langmuir and Freundlich constants, and n is the adsorption strength.

In the kinetic adsorption experiments, AC (10 mg) was added to 200 mL (170 μmol $L^{-1}$) of $Cu^{2+}$ solution. The conical flask was placed on a thermostatic shaker (250 rpm). After shaking for 5, 10, 15, 30, 60, 90, 120, 150, 180 min, the post-sorption concentration of $Cu^{2+}$ was measured by UV spectrophotometer AC. Fitting was performed by using pseudo-first-order (equation S4) and pseudo-second-order

kinetic models (equation S5).

$$\ln(Q_e-Q_t)=\ln Q_e-k_1 t \qquad S(4)$$

$$t/Q_t=1/k_2 Q_e^2+t/Q_e \qquad S(5)$$

where $Q_t$ (mg $g^{-1}$) is adsorption capacity at a specific time, $k_1$ is the rate constant of the pseudo-first-order and $t$ (min) is adsorption time.

The internal diffusion model considers that the adsorbate diffuses from the outer surface of the adsorbent and enters into the inner surface through the pores on the adsorbent particles. The rate of this step mainly depends on the adsorbate diffuses speed through the pore, which is shown in the equation S(6).

$$Q_t=K_{id}t^{1/2} \qquad S(6)$$

where $K_{id}$ is the internal diffusion rate constant, mg $g^{-1}\cdot min^{1/2}$.

If the relation between the $Q_t$ and $t^{1/2}$ was in a straight line, there would be an internal diffusion process during the adsorption process.

**Measurement of quantum yield (QY)**

The relative QY of the CQDs can be calculated by equation S(7) as follow:

$$\Psi_x=\Psi_s \times (I_x A_s \eta_x^2)/(I_s A_x \eta_s^2) \qquad S(7)$$

Where $\Psi$ is the fluorescence QY, x and s represent the test substance and the reference compound, $\eta$ is the refractive index (1.33 for aqueous solution, ethanol is 1.003), $A$ is the absorbance at an excitation wavelength of 360 nm, $I$ is the integrated fluorescence intensity under the fluorescence emission spectrum. To reduce the interference of the reabsorption effects, the absorbance at excitation 360 nm was controlled to 0.01-0.1.

**Fluorescence quenching principle**

The fluorescence quenching mechanisms are classified into static burst mechanism and dynamic burst mechanism to explain the fluorescence burst. The Stern-Volmer equation can be utilized as a basis for discrimination of quenching phenomenon of the CQDs fluorescence caused by $Cu^{2+}$, as described the following:

$$F_0/F=1+K_{SV}[C] \qquad S(8)$$

where $F_0$ and F are the fluorescence intensities of CQDs suspensions without and with $Cu^{2+}$ ions at the optimal excitation wavelength of 360 nm, respectively, $K_{SV}$ is the

Stern-Volmer burst constant, and [C] is the concentration of $Cu^{2+}$.

The slope of this plot was $K_{SV}$=0.012782 $nm^{-1}$. For the dynamic quenching effect, $K_{SV}$ is proportional to the fluorescence lifetime. For the dynamic burst effect, $K_{SV}$ is proportional to fluorescence lifetime [1].

$$K_{SV}=K_q t_0 \qquad S(9)$$

where $K_q$ is the bimolecular quenching constant, the average fluorescence lifetime ($\tau_0$) and $K_{SV}$ value (0.013 $nm^{-1}$) of CQDs without the presence of $Cu^{2+}$ (1.06 ns) were used. So the bimolecular burst constant ($K_q$) value was found to be $1.21\times10^{11}$ $M^{-1}s^{-1}$, indicating that it was static quenching rather than dynamic quenching because the rate constant for dynamic quenching is generally considered to be less than $1.0\times10^{10}$ $M^{-1}s^{-1}$ [2].

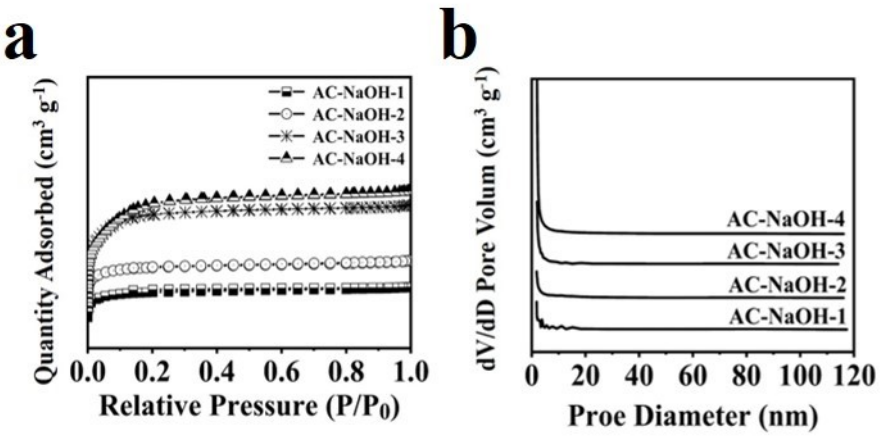


**Fig. S1** (a) Nitrogen adsorption-desorption isotherms and, (b) pore size distribution

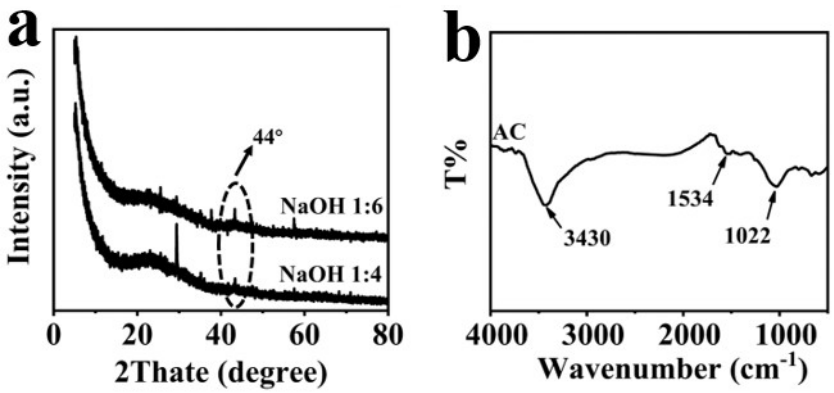


**Fig. S2** (a) X-ray diffraction patterns of AC-NaOH-3 and AC-NaOH-4 (b) FT-IR of AC-NaOH-4

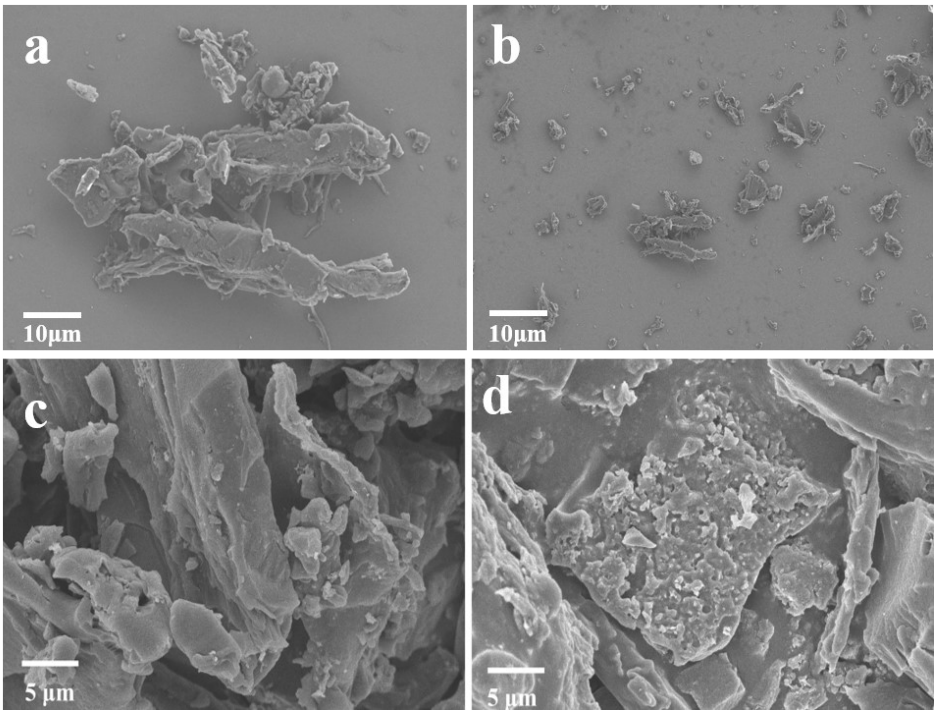


**Fig. S3** SEM images of bare wolfberry stems (a, b) and (c, d) AC-NaOH-3, AC-NaOH-4

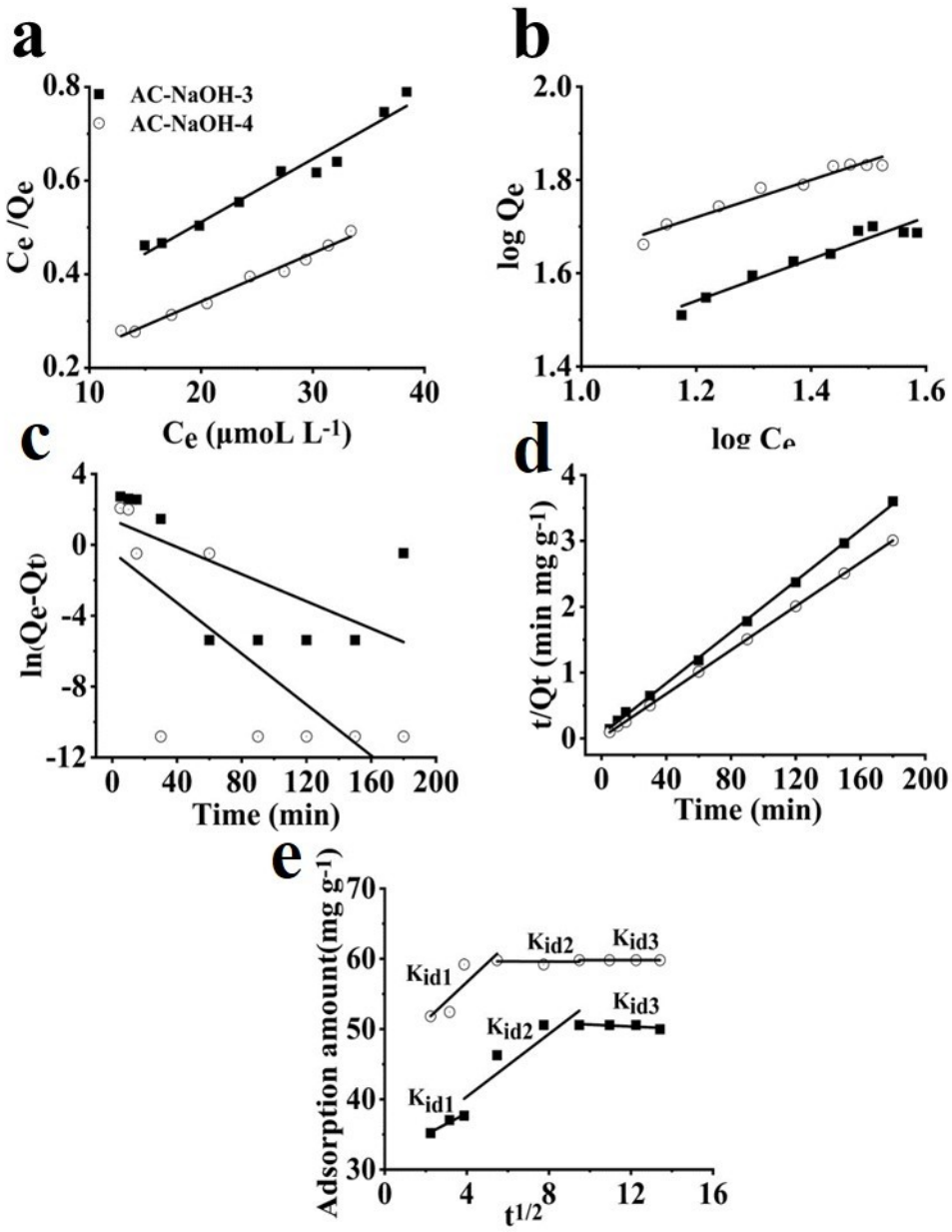


**Fig. S4** Fitting of (a) Langmuir adsorption model, (b) Freundlich model to isothermal adsorption, (c) pseudo-first-order, (d) pseudo-second-order and (e) internal diffusion adsorption model fitting to kinetic adsorption curves

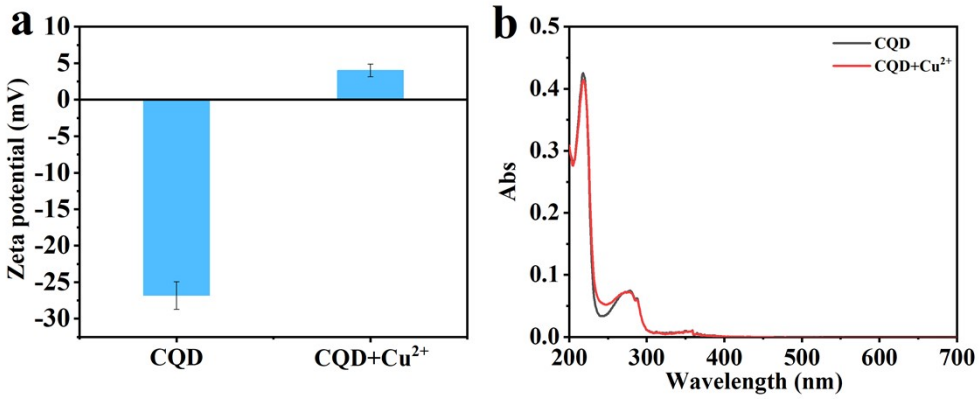


**Fig. S5** Zeta potential (a) of CQDs alone, and CQDs with the addition of $Cu^{2+}$ metal ions, and UV spectra(b) of CQDs alone, and after addition of $Cu^{2+}$ ions.

**Table S1** Comparison of wolfberry stem-based AC with other biomass-derived AC

| Precursor materials | Activator | Temperature (℃) | $S_{BET}$ ($m^2 \cdot g^{-1}$) | Ref. |
|---|---|---|---|---|
| Microalgae | Water vapor | 800 | 785 | [21] |
| Termite biodiesel | KOH | 900 | 1465 | [22] |
| Palm date seeds | $CO_2$ | 900 | 2344 | [23] |
| wolfberry stem | NaOH | 600 | 3016 | This work |

**Table S2** Adsorption isotherm parameters of $Cu^{2+}$ on AC-NaOH-3 and AC-NaOH-4 by Langmuir and Freundlich models

| Adsorbent | Langmuir model | | | Freundlich model | | |
|---|---|---|---|---|---|---|
| | $K_L$ (L·mg$^{-1}$) | $Q_M$ (mg·g$^{-1}$) | R | $K_F$ (mg·g$^{-1}$) | n | R |
| NaOH (1:4) | 0.056 | 72.99 | 0.988 | 10.06 | 2.23 | 0.566 |
| NaOH (1:6) | 0.076 | 96.89 | 0.993 | 17.34 | 2.49 | 0.797 |

**Table S3** Kinetic parameters of $Cu^{2+}$ adsorption on AC-NaOH-3 and AC-NaOH-4 by pseudo-first-order and pseudo-second-order models

| Sample | pseudo-first-order | | pseudo-second-order | | | Internal diffusion | | |
|---|---|---|---|---|---|---|---|---|
| | $K_1$ ($min^{-1}$) | $R_1$ | $Q_e$ ($mg \cdot g^{-1}$) | $K_2$ ($g\ mg^{-1}\ min^{-1}$) | $R_2$ | $k_{id1}$ | $k_{id2}$ | $k_{id3}$ |
| NaOH (1:4) | 0.0383 | 0.566 | 51.54 | $6\times10^{-4}$ | 0.999 | 1.52 | 1.11 | -0.24 |
| NaOH (1:6) | 0.0719 | 0.754 | 60.24 | $4\times10^{-4}$ | 0.999 | 4.32 | 0.056 | -6.75 |

**Table S4** Correlation of adsorption capacity of AC on $Cu^{2+}$

| Precursor materials | Activator | Adsorption equilibration time (min) | Adsorption capacity (mg $g^{-1}$) | Ref. |
|---|---|---|---|---|
| Wheat Straw | KOH | 200 | 57.5 | [32] |
| Walnut Shell | $CO_2$ | 40 | 32 | [33] |
| Pinewood | $H_3PO_4$ | 40 | 20 | [29] |
| Wolfberry stems | NaOH | 30 | 59 | This work |

Table S5 Actual water sample adsorption (AC=10 mg V=50 mL)

| | Preadsorption concentration (mg $L^{-1}$) | Adsorption concentration (mg $L^{-1}$) | Adsorption capacity (mg $g^{-1}$) |
|---|---|---|---|
| $Cu^{2+}$ | 12.8 | 0.068 | 63.66 |
| $Fe^{3+}$ | 11.2 | 0.518 | 53.41 |
| $Cr^{6+}$ | 10.4 | 0.518 | 49.41 |
| $K^{+}$ | 7.8 | 2.822 | 24.89 |
| $Na^{+}$ | 4.6 | 2.089 | 12.55 |
| $Ca^{2+}$ | 4 | 2.799 | 6.00 |

**Reference**

[1] G.K. Hu, L. Ge, Y.Y. Li, M. Mukhtar, B. Shen, D.S. Yang, J.G. Li, Carbon dots derived from flax straw for highly sensitive and selective detections of cobalt, chromium, and ascorbic acid, Journal of Colloid and Interface Science, 579 (2020) 96-108.

[2] S.Y. Tang, D. Chen, G.Q. Guo, X.M. Li, C.X. Wang, T.T. Li, G. Wang, A smartphone-integrated optical sensing platform based on Lycium ruthenicum derived carbon dots for real-time detection of $Ag^{+}$, Science of the Total Environment, 825 (2022).